J Mater Sci (2020) 55:6093–6104

Materials for life sciences

Nitrogen and sulfur co-doped carbon nanodots in living EA.hy926 and A549 cells: oxidative stress effect and mitochondria targeting

Zuowei Ji[1], Durga M. Arvapalli[1], Wendi Zhang[1], Ziyu Yin[1], and Jianjun Wei[1,*]

[1] *Department of Nanoscience, Joint School of Nanoscience and Nanoengineering, University of North Carolina at Greensboro, Greensboro, NC 27401, USA*

Received: 11 November 2019
Accepted: 31 January 2020
Published online: 6 February 2020

ABSTRACT

Carbon nanodots (CNDs) have been studied in the field of biomedicine, such as drug delivery, bioimaging and theragnosis because of their superior biocompatibility and desirable optoelectronic properties. However, limited assessments on the biological effects of CNDs, particularly the effect on oxidative stress and toxicity in living cells, are not adequately addressed. In this work, a type of nitrogen, sulfur-doped carbon nanodots (N,S-CNDs), which were found to have strong antioxidant capacity in free radical scavenging in physicochemical conditions, was investigated through measuring the fluctuations of the intracellular reactive oxygen species (ROS), such as the hydrogen peroxide and superoxide anion, at different dose exposure in two types of cell lines, EA.hy926 and A549 cells. Instead of showing antioxidative capacity, the results indicate the uptake of the N,S-CNDs induces the production of intracellular ROS, thus causing oxidative stress and deleteriousness to both cell lines. The mitochondrial membrane potential of the cells was monitored upon the N,S-CNDs treatment and found to increase monotonically with the concentration of the CNDs. In addition, the confocal imaging of the cells confirms the localization of the CNDs at the mitochondria. More evidence suggests that the N,S-CNDs may stimulate ROS generation by interacting with the electron transport chain in the mitochondrial membrane due to the sulfur composite in the CNDs.

Introduction

The engineered nanoparticles (NPs) have been widely used in cosmetics, sensors, optoelectronics and will be increasingly applied in the diagnostic and therapeutic fields, e.g., bioimaging and drug delivery [1–6]. The NPs currently under development for biomedical applications have been mainly divided into three categories according to the composites: (1) metal-based NPs, e.g., gold or silver NPs, (2)

Address correspondence to E-mail: j_wei@uncg.edu

https://doi.org/10.1007/s10853-020-04419-7

semiconductor-based NPs, i.e., semiconductor quantum dots (QDs) and (3) carbon-based NPs [5], such as fullerenes, and single- or multi-walled carbon nanotubes, and carbon nanodots (CNDs). One of the critical properties of NPs in biomedical applications is the cytotoxicity and biocompatibility [7]. In terms of carbon-based NPs, single-walled carbon nanotubes (SWNTs) showed that both oxidative stress and inhibition of proliferation increased in a time- and dose-dependent manner in various cell lines [8]. Studies on multi-walled carbon nanotubes (MWNTs) by Monteiro-Riviere et al. [9] yielded results similar to those of SWNTs. Since the oxidative stress effect and cytotoxicity of NPs are suggested to be related to various parameters of NPs, such as size difference [10], surface coating [11], chemical composition [12] and nanoparticle aggregation [13, 14], it is necessary and vital to conduct and examine the biological interactions and resultant cytotoxic effects for each type of NPs.

Carbon nanodots (CNDs) have drawn extensive attention owing to their easy-to-synthesis [15], superior biocompatibility and outstanding optoelectronic properties [16] since the discovery in 2004 [17]. CNDs have been researched for applications in the field of biomedicine, sensors, optoelectronics and catalysis [18–23]. Recently, our group and others showed antioxidant capacity of CNDs on scavenging free radicals in both physicochemical [24–26] and in vitro environments [27–30]. For examples, Das et al. [27, 28] have reported the reactive oxygen species (ROS) scavenging capability of the biomass-derived carbon dots both in vitro and in vivo. Durantie and his co-workers claimed no harmful effects induced by 24 h CNDs incubation at concentration of 0.1 mg/mL on cells assessed by cytotoxicity, oxidative stress and other parameters [31]. On the other hand, a few reports suggest dual antioxidant and prooxidant properties of CNDs depending on the source for CND synthesizing and external conditions (e.g., light excitation) [32, 33]. CNDs were also reported toxicity at relative high concentration [34]. As a fact, literature data concerning such biological properties of CNDs and the underlying reactions are yet limited. There are just few studies of CNDs on the oxidative stress in cells. Havrdova et al. [35] reported different levels of intracellular ROS increment induced by three types of carbon dots with different surface coating to tune surface charges. It becomes essential to assess the potential consequence of CNDs in living cells in order to guarantee their safe development for biomedical applications.

More recently, we reported a type of nitrogen, sulfur-doped CNDs (N,S-CNDs) that demonstrate improved antioxidant capacity in scavenging free radicals, such as 2,2-diphenyl-1-picrylhydrazyl radical ($DPPH^{\cdot}$), and inhibition of ROS produced through the xanthine/xanthine oxidase (XO) reaction in physicochemical environment [24]; none of these experiments are performed in cells. How the N,S-CNDs perform in living cells is a question and unknown. Based on the discoveries in [24], we moved our study from physiochemical settings further into in vitro cellular level. Cellular studies have been widely accepted to investigate how an agent reacts in a biological system at the cellular and even molecular levels. The cells' reaction can be examined in a relatively easy-controlled environment. Herein, we present new findings of the N,S-CNDs in terms of the effect on the oxidative stress in living cells. Because different types of CNDs could trigger distinctive biological responses in cell lines, we propose to assess the effect on oxidative stress of the N,S-CNDs in two cell lines, EA.hy926, a normal human umbilical vein cell line, and A549, an adenocarcinomic human alveolar basal epithelial cell line. This research design offers an opportunity to compare the treatment of N,S-CNDs in normal cells and malignant cells. Based on the physicochemical experiment results, the in vitro experiments are performed at a range of 0.05–0.8 mg/mL doses of N,S-CNDs. Contrast to reported effect against oxidative stress on cells of the same level of nitrogen-doped CNDs [36], the N,S-CNDs show in vitro toxicity and induce the intracellular ROS generation, rather than scavenging ROS radicals. The ROS production is ascribed to the interactions between the N,S-CNDs and mitochondria in cells, which is corroborated by mitochondria membrane potential measurement and mitochondria targeting imaging.

Materials and methods

CND synthesis and characterization

The synthesis of the N,S-CNDs was performed using a hydrothermal method from precursor molecules of α-lipoic acid + citric acid + and urea, which has been previously reported in details [24]. The purified

N,S co-doped CNDs were characterized using transmission electron microscopy (Libra 120 PLUS TEM, Carl Zeiss) and atomic force microscopy (5600LS AFM, Agilent) for the size and morphology evaluation. The CNDs were dispersed on a mica surface for AFM and a cooper grid for the TEM measurements. The structure and composites of CNDs were characterized by Fourier transform infrared spectroscopy (670 FTIR, Varian), Raman spectroscopy (XploRA ONE, Horiba) and X-ray photoelectron spectroscopy (ESCALAB 250Xi XPS, Thermo Fisher). The absorption spectrum was measured using a UV–Vis photospectrometer (Cary 6000i, Agilent), and fluorescence was measured using a fluorometer (Cary Eclipse, Agilent). Zeta potential of the N,S-CNDs dissolved in DI water (~ 0.05 mg/mL) was measured by a Malvern Zetasizer nano-ZX (Malvern Instruments ZEN3600).

Cell culture

EA.hy926 endothelial cells purchased from ATCC (Manassas, VA) were cultured with optimized DMEM (AddexBio, C0003-02) media containing 1% streptomycin–penicillin (Fisher Scientific) and 10% fetal bovine serum (Sigma-Aldrich) at 37 °C in a 5% CO_2 humidified incubator. Human lung epithelial cell line A549 (ATCC, CCL-185) was cultured in F-12K (Kaighn's Modification of Ham's F-12 medium) (ATCC, 30-2004) medium supplemented with 10% fetal bovine serum (Sigma-Aldrich) and 1% streptomycin–penicillin (Fisher Scientific) in a cell culture-treated flask at 37 °C in a 5% CO_2 humidified incubator.

3-(4,5-Dimethylthiazol-2yl)-2,5-diphenyltetrazolium bromide (MTT)-based assay

Briefly, cells were firstly plated in a tissue culture-treated 24-well plate with a density of 0.5×10^5 per well. After 24 h incubation, the medium was replaced with the N,S-CND suspensions in new complete media at different doses (0.05–0.8 mg/mL) for 24 h. After the exposure, the CNDs suspensions were discarded and a 500 µL complete medium solution containing 0.2 mg/mL MTT (99%, Fisher Scientific) was added and incubated for additional 2 h. Then, the MTT solution was removed and a 500 µL DMSO solvent was added to dissolve the formazan crystal for 5 min at room temperature after rinsing with phosphate buffer solution (PBS). The absorbance of each well was quantified using a BioTek microplate reader at wavelength of 570 nm.

Intracellular reactive oxygen species (ROS) measurement

Firstly, the cells were plated in the 96-well plate with a cell density of 1×10^4 and incubated for 24 h. Then the medium was removed, and the N,S-CNDs suspensions at different concentrations (0.1–0.8 mg/mL) were added. After 24 h exposure, the particle suspensions were discarded, and the cells were rinsed twice with PBS. Thereafter, 10 µM and 40 µM 2′,7′-dichlorofluorescin diacetate (DCFH-DA, Sigma-Aldrich) diluted in FBS-free media was added to EA.hy926 endothelial cells and A549 cells, respectively, and the cells were incubated for additional 30 min. The DCFH-DA was then removed, and the cells were rinsed twice with a 100 µL PBS. Finally, 100 µL PBS was added into each well, and fluorescence of each well was measured by a BioTek microplate reader with excitation/emission at 485/528 nm. Following CNDs' fluorescence background subtraction, the data were represented by histogram. In parallel, treatment of cells with same concentrations of L-ascorbic acid (AA) was used as a negative control.

Intracellular superoxide anion measurement

Cells were firstly plated on glass cover slips with a cell density of 1×10^5 inside a 12-well tissue culture plate for 24 h. Then, the cells were treated with the N,S-CNDs suspensions at 0.4 mg/mL and 0.8 mg/mL for 24 h, respectively. A 0.4 mg/mL AA was used as a negative control. After exposure, cells were washed twice with PBS and incubated with dihydroethidium (DHE) for 30 min at concentration of 10 µM. Cover slips with cells were again rinsed twice with PBS and transferred immediately to a Zeiss Z1 Spinning Disk Confocal for the live cell imaging under rhodamine (RHOD) channel. Micrographs were collected from at least 10 different regions of each sample. The background fluorescence was obtained from a cell-free field in each image and subtracted from the actual fluorescence.

Measurement of mitochondrial membrane potential (ΔΨm) and imaging subcellular localization of N,S-CNDs

The ΔΨm was measured using MitoTracker Red CMXROs (Invitrogen). Firstly, cells were seeded on glass cover slips inside a 12-well tissue culture plate with a cell density of 1×10^5. After incubation for 24 h, the N,S-CNDs suspensions at concentration of 0.4 mg/mL and 0.8 mg/mL were added to the cells, respectively, and incubated for additional 24 h. After the N,S-CNDs treatment, cells were rinsed with PBS and incubated with FBS-free medium containing MitoTracker Red CMXRos (0.2 μM for EA.hy926 cells and 0.1 μM for A549 cells) for 10 min at 37 °C. Afterward, the cells were washed twice with PBS to remove excess dye and immediately imaged by a Zeiss Z1 Spinning Disk Confocal under RHOD channel. Micrographs were collected from at least 10 different loci of each sample. The background fluorescence was obtained from a cell-free field in each image and subtracted from the actual fluorescence. Moreover, the cells were imaged under RHOD and DAPI channel at the same time to track the localization of the N,S-CNDs.

Statistical analysis

Results were expressed as means ± standard deviation (SD) from at least three independent experiments. Differences at $p < 0.05$ were considered significant in histograms. Fluorescence intensity from confocal micrographs was analyzed using Axiovision 4.8 software. The quantified fluorescence intensities in histograms were obtained by subtracting the background fluorescence from the actual fluorescence in each micrograph.

Results

Nitrogen, sulfur-doped CNDs (N,S-CNDs)

N,S-CNDs were synthesized using a reported hydrothermal method from precursor molecules α-lipoic acid, citric acid and urea [24]. After synthesis and purification, the characterization of CNDs was carried out using atomic force microscopy (AFM), Fourier transform infrared spectroscopy (FTIR), Raman spectroscopy, X-ray photoelectron spectroscopy (XPS), Zeta potential, UV–Vis spectroscopy and fluorescence spectroscopy. More detailed morphology and structure–property information was described in our recent publication [24]. In brief, the N,S-CNDs have a spherical morphology with size of averaged 3 nm measured by TEM and the height profile analysis from AFM imaging (Fig. S1). Note that, since the radius of the curvature of the AFM tip is much bigger than CNDs, the *X*, *Y* image size is not the actual size of the CNDs. The *Z* profile has nanoscale resolution and is used to obtain the size of CNDs. The N,S-CNDs possess multiple surface functional groups of carboxylates, amines/amides and thiol/sulfide, and different types of bonds, such as C–C, C–N, C–S, C–O, C=C, C=O, C=N, O=C–OH, which are identified by FTIR, Raman spectroscopy (Fig. S2) and X-ray photoelectron spectroscopy (XPS). Specifically, the S 2*p* XPS spectrum verifies two doublets at ~ 165 (C–S S2*p*1/2), 163.7 (C–S S2*p*3/2), 163.0 (S2–S2*p*1/2) and 161.7 (S2–S2*p*3/2) eV. The full XPS survey and spectra of C 1*s*, O 1*s*, N 1*s* and S 2*p* are shown in (Fig. S3–S7). The estimated element percentage in the N,S-CNDs is C1*s* (78.2%), O1*s* (10.5%), N1*s* (6.6%) and S2*p* (4.7%), respectively. Zeta potential of the N,S-CNDs in DI water (~ 1 mg/mL) at room temperature was measured to be − 0.07 ± 4.17 mV (Fig. S8). The optical property is critical for imaging in cells. Figure 1 displays the absorption and fluorescence spectra. The band around 270 nm in the absorption spectrum (Fig. S7A) can be assigned to the π–π* transition of C=N bonds (sp^2 domains) [37, 38] and the absorbance feature between 300 and 350 nm can be ascribed to intra-transitions of surface states [39, 40]. Unlike the previous N,S co-doped CNDs synthesized from precursors citric acid (CA) and L-cysteine [40], our N,S-CNDs present excitation-dependent fluorescence primarily because of the different precursor molecules resulting in more surface states as origin of the fluorescence [41]. The relative quantum yield of fluorescence using a quinine sulfate reference at 340 nm excitation was obtained to be 11.4 ± 0.6%.

Cell viability

The biocompatibility of the N,S-CNDs was firstly evaluated by MTT (3-(4,5-dimethyl thiazol-2-yl)-2,5-diphenyl tetrazolium bromide) assay, which is a colorimetric metabolic assay. Concretely, the mitochondria of viable cells are capable to reduce the

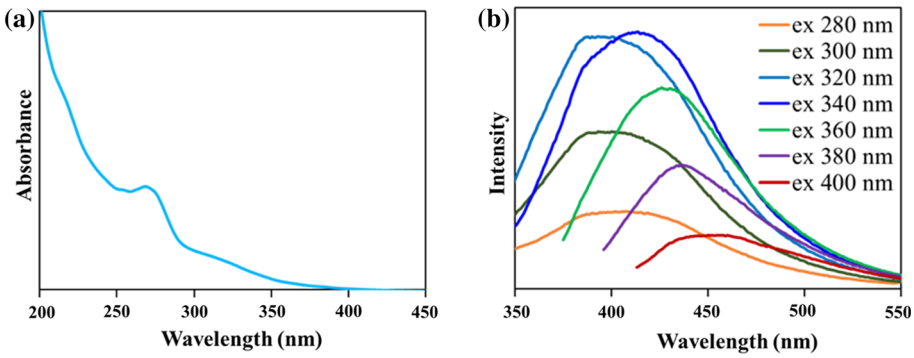

Figure 1 **a** Absorption spectrum and **b** fluorescence emission spectra of the N, S co-doped CNDs in deionized water.

yellow soluble MTT into a purple insoluble formazan product, which could be dissolved by dimethyl sulfoxide (DMSO) and quantified by measuring the absorbance at 570 nm with a microplate reader [42]. Consequently, the viability of the cells could be assessed. Here, the cytotoxicity parameter of CNDs was determined using EA.hy926 endothelial cells and human lung adenocarcinoma A549 cells, respectively. As shown in Fig. 2a, statistical significance in reduction of cell viability was observed with increasing concentrations of CNDs. Statistically, the viability of EA.hy926 decreased to 53% after 24 h incubation with 0.8 mg/mL N,S-CNDs. For comparison, A549 cell line demonstrated similar growth inhibition pattern, but a lesser extent than EA.hy926 endothelial cell line after N,S-CNDs treatment. Figure 2b shows that 60% viability of A549 cells was observed after 0.8 mg/mL N,S-CNDs' exposure. Collectively, these results indicate that the EA.hy926 cells are more sensitive to the treatment of CNDs than A549 cells.

Quantification of the intracellular ROS production

The growth inhibition effects on cells of the N,S-CNDs led us to the assessments of the intracellular ROS generation since some researchers have attributed the in vivo and in vitro toxic effects of nanomaterials to the generation of ROS and the induction of oxidative stress [43, 44]. The so-called ROS, much of which generates in the mitochondria, are highly reactive oxygen containing by-products of cellular oxidative metabolism, including hydrogen peroxide (H_2O_2), superoxide ion (O_2^-) and hydroxyl radical (OH^-), [45, 46]. The role of ROS in cellular processes is kind of resembling double-edged swords. On the one hand, ROS that serve as specific signaling

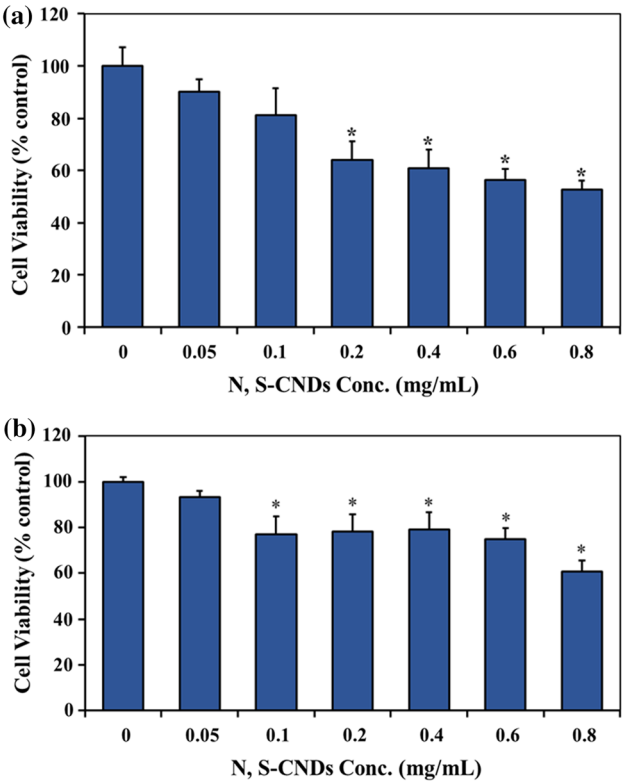

Figure 2 Viability of EA.hy926 endothelial cells (**a**) and A549 cells (**b**) after 24-h exposure of the N,S-CNDs evaluated by MTT assay at indicated concentrations. Values are shown as mean ± SD from three independent experiments. *Denotes a significant difference from the control (0 mg/mL) ($p < 0.05$).

molecules are essential to maintain homeostasis under normal physiological conditions [47–49]. On the other hand, overproduction of ROS could cause damage to many biomolecules in cells including lipids, proteins and nucleic acids due to its high reactivity, which will result in diseases and aging [50–52].

Therefore, monitoring the fluctuation of intracellular ROS level becomes very necessary when we are

assessing the cytotoxicity. To this end, we evaluated the intracellular ROS production, especially hydrogen peroxide (H_2O_2), using oxidation-sensitive fluoroprobe DCFH-DA by a microplate reader in both EA.hy926 and A549 cells. DCFH-DA is a nonfluorescent and cell-permeable compound which could be hydrolyzed intracellularly by esterases to the carboxylate anion (DCFH). DCFH is then oxidized to fluorescent dichlorofluorescin (DCF) by cellular oxidants, which could be detected by confocal microscopy or microplate reader. The intensity of the fluorescence thereby indicates intracellular ROS (hydrogen peroxide) level. Figure 3a and b exhibits a dose-responsive DCF fluorescence in EA.hy926 cells and A549 cells, respectively, with treatment of the N,S-CNDs. Note that, the fluorescence intensity is normalized with respect to the intensity without CND treatment. The cells treated with L-ascorbic acid (AA), which is known as an inhibitor of ROS generation [53, 54], were performed in parallel as negative controls for comparison. The increment of ROS in EA.hy926 cells is more significant than that in A549 cells with increasing the concentration of N,S-CNDs. Specifically, the increase in fluorescence signal is insignificant within the range of 0.1–0.4 mg/mL for A549 cells, and significant difference was observed at 0.6 and 0.8 mg/mL compared to the untreated cells. It should be noted that the results in this ROS assay agree with the results from MTT assay, which suggest certain level of cytotoxic effect of the N,S-CNDs is related to the ROS generation.

Visual detection of intracellular superoxide anion (O_2^-)

Superoxide (O_2^-), one key member of ROS, is one of the primary by-products of the partial reduction of O_2 during aerobic metabolism [55, 56]. Dihydroethidium (DHE), also called hydroethidine (HE), was used specifically to indicate intracellular O_2^- in this study. DHE is cell permeable and could be intracellularly oxidized to ethidium (E^+), which could intercalate within the cell's DNA, staining its DNA with a bright fluorescent red. Therefore, the intracellular level of O_2^- could be visually inspected by confocal microscopy. The concentrations of N,S-CNDs at 0.0, 0.4, 0.8 mg/mL were used for the cell treatment. Figure 4 shows an positive correlation between the fluorescence intensity of DHE in both EA.hy926 cells and A549 with the N,S-CNDs' concentration. The quantified fluorescence signal was shown in Fig. 4i1–2. AA was served as a negative control here (Fig. 4g–h). The intensity increase at 0.4, 0.8 mg/mL N,S-CNDs treatment indicates the O_2^- generation in EA.hy926 cells (Fig. 4a1–f1). In the case for A549 cells, strong fluorescence enhancement was observed after 0.8 mg/mL CNDs' exposure, while less DHE signal increase was observed between untreated A549 cells and 0.4 mg/mL CNDs' treatment (Fig. 4a2–f2). Figure 4i2 indicates the quantification of the fluorescence intensity in A549 cells. These observations suggest that EA.hy926 cells are more sensitive to the N,S-CNDs in terms of the induction for ROS generation at low concentration (0.4 mg/mL) but no significant difference at higher concentration (0.8 mg/mL). Overall, the results from this assay demonstrate a dose-dependent increment of intracellular O_2^- with increasing concentrations of CNDs in both cell lines.

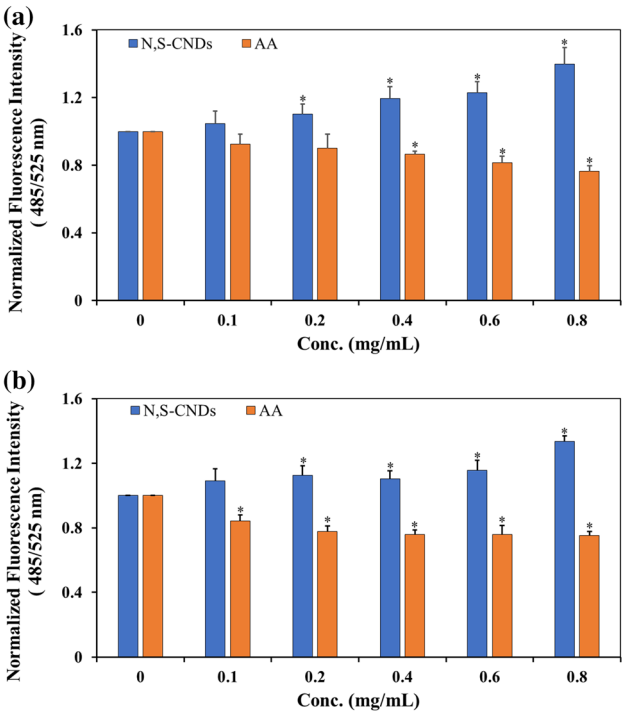

Figure 3 Effects of CNDs on intracellular ROS production. ROS (H_2O_2) generation in EA.hy926 endothelial cells (**a**) and A549 cells (**b**) treated with CNDs for 24 h was monitored by the addition of DCFH-DA probe. The fluorescence in the cells was quantified by a microplate reader. Values are shown as mean ± SD from three independent experiments. Triplicates of each treatment were performed in each independent experiment. *$p < 0.05$ versus control (0 mg/mL).

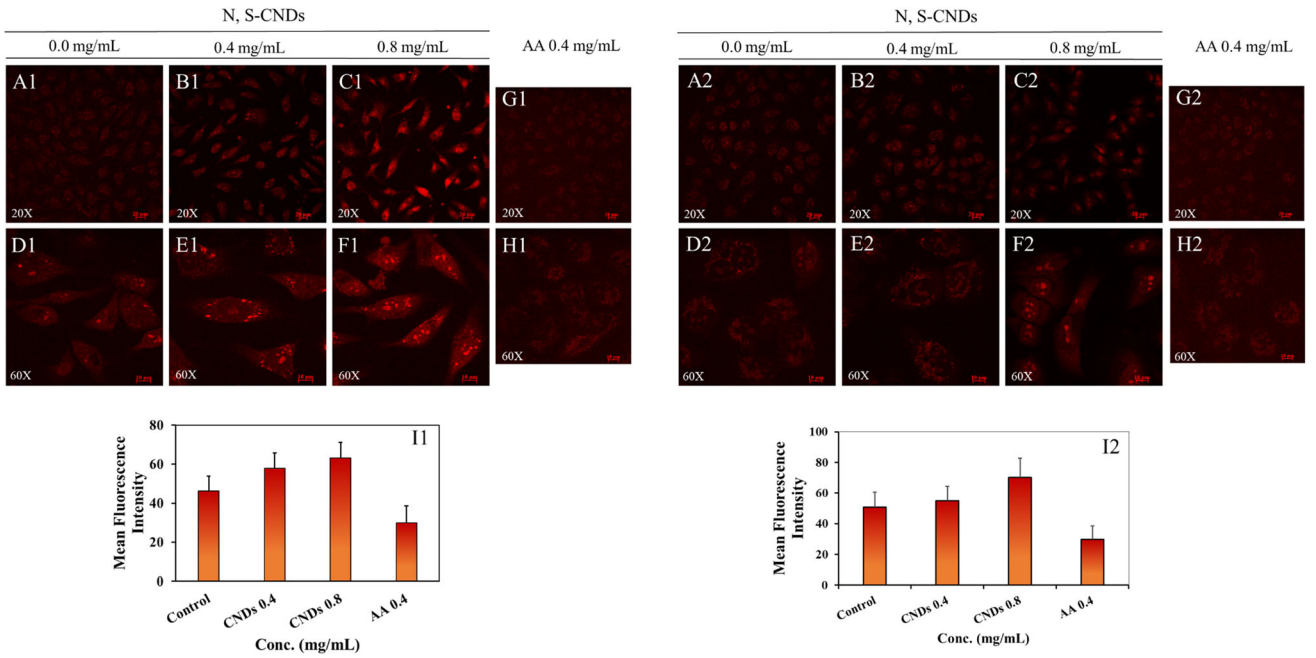

Figure 4 Visualization and image-based quantification of the N,S-CNDs-induced O_2^- generation in EA.hy926 cells (left) and A549 cells (right). Micrographs (**a**, **b**, **c**) show the fluorescence of indicator DHE in the two cell lines treated with 0.0, 0.4 and 0.8 mg/mL N,S-CNDs under RHOD channel with magnification of 20 ×, respectively; micrographs (**d**, **e**, **f**) show the fluorescence of indicator DHE in two cell lines treated with same concentrations under RHOD channel with magnification of 60 ×. AA (L-ascorbic acid) treatment of the cells serves as a negative control (**g**, **h**). Histogram (**i1–2**) presents the quantified fluorescence intensity of 10 different regions in each treatment.

Mitochondrial membrane potential (ΔΨm) and imaging of CND's subcellular locations

Mitochondria have been considered as the main loci for the production of ROS [57, 58]. Moreover, the concept that higher ΔΨm is associated with more generation of ROS has been widely accepted [59, 60]. This in turn leads us to the investigation of the change of ΔΨm before and after the CNDs' treatment, thus to test the hypothesis that the intracellular process of the N,S-CNDs stimulates mitochondria activity in ROS production. For this purpose, MitoTracker Red was used to stain mitochondria in live cells and its accumulation is dependent upon membrane potential. The fluorescence intensity increases positively with the membrane potential which can be monitored by confocal microscopy imaging. Figure 5a1–f1 presents the confocal images of the EA.hy926 upon treatment of 0.0, 0.4 and 0.8 mg/mL N,S-CNDs. The ΔΨm of EA.hy926 elevated accordingly after the CNDs' treatment based on the increment of quantified fluorescence intensity (Fig. 5g1). In addition, no unusual conformational changes of the mitochondria were observed after CNDs treatments. In the case of A549 cell line, a significant enhancement of ΔΨm was observed after 0.8 mg/mL CNDs' exposure (Fig. 5c2), while no obvious change was found at the concentration of 0.4 mg/mL (Fig. 5b2). The quantification of the fluorescence signal is presented in Fig. 5g2. And similarly, the morphology of mitochondria of A549 did not show much difference before and after CNDs treatments (Fig. 5d2–f2).

To observe the subcellular location of N,S-CNDs, cells were treated with the CNDs for 24 h (0.8 mg/mL) and then incubated with MitoTracker (1 μM). The localization of the CNDs in the subcellular level was observed by merging the MitoTracker images with the CNDs confocal images. Figure 6 clearly displays the confocal images of the two cells. The red fluorescence is attributed to the MitoTracker (Fig. 6a1, b1), and the blue fluorescence is ascribed to the N,S-CNDs (Fig. 6a2, b2). The merged channel (Fig. 6a3, b3) of the CNDs-MitoTracker shows good co-localization of CNDs-MitoTracker to the mitochondria. The 3D images of individual cells clearly show the overlap of the red and blue color at the mitochondria area. A more quantitative subcellular

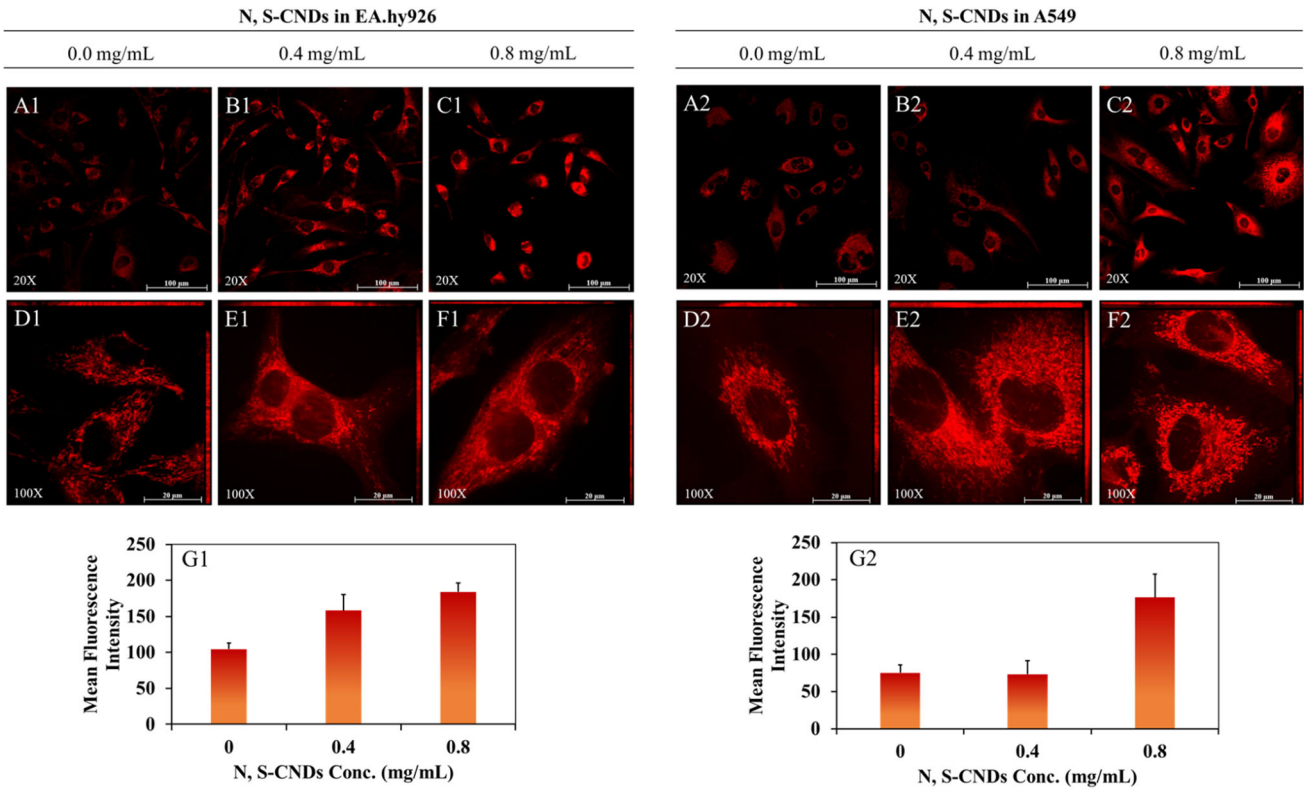

Figure 5 Visualization and image-based quantification of CNDs-induced ΔΨm change in EA.hy926 cells and A549 cells. Micrographs (**a**, **b**, **c**) exhibit the MitoTracker Red CMXROs fluorescence in cells treated with 0.0, 0.4 and 0.8 mg/mL N,S-CNDs under RHOD channel with magnification of 20 ×, respectively; micrographs (**d**, **e**, **f**) exhibit the MitoTracker Red CMXROs fluorescence (Ex: 638 nm) in cells treated with 0.0, 0.4 and 0.8 mg/mL CNDs under RHOD channel with magnification of 100 ×, respectively. Histogram (**g**) reveals the averaged fluorescence intensity of 10 different loci picked in each treatment (15 points of each locus for a total ∼ 150 data points).

location of the N,S-CNDs in the cells was analyzed using Pearson's correlation coefficient from the correlation plots with MitoTracker red images (Fig. S8). The coefficient values for the CNDs-MitoTracker group were 0.70 and 0.63 in EA.hy926 and A549 cells, respectively, suggesting a strong positive linear-relationship, thus the staining of mitochondria by the N,S-CNDs. This mitochondrial targeting ability is consistent with reports using CNDs possessing similar surface functional groups, such as $–COO^-$, $–NH_3^+$, –OH and –C–SH [61, 62]. The ability of N,S-coped CNDs for selective mitochondria targeting can be explained by the surface functional groups, especially the positive charged groups (e.g., $–NH_3^+$) which interact with negatively charged cell membrane thus facilitating cell translocation into cytosol through endocytosis mediated passive diffusion [63, 64].

Discussion

Taken together, these results indicate that the N,S co-doped CNDs induced more generation of ROS not only in normal cells but also in cancer cells at the dose range of 0.2–0.8 mg/mL in this work. More specifically, the normal human umbilical vein cell line, EA.hy926, is more sensitive to the N,S-CNDs at relative lower concentration (< 0.6 mg/mL) than the A549 human lung adenocarcinoma cell line, and consistent in observations from the MTT assay for viability, ROS production (both H_2O_2, superoxide ion O_2^- measurement), as well as the mitochondrial membrane potential. The A549 cell line has propensity of ROS generation more likely at relative high concentration (0.8 mg/mL) of the N,S-CND treatment rather than low concentration. The difference of the responses from the two cell lines might be explained by the microenvironment during intracellular process and regulation with the mitochondria

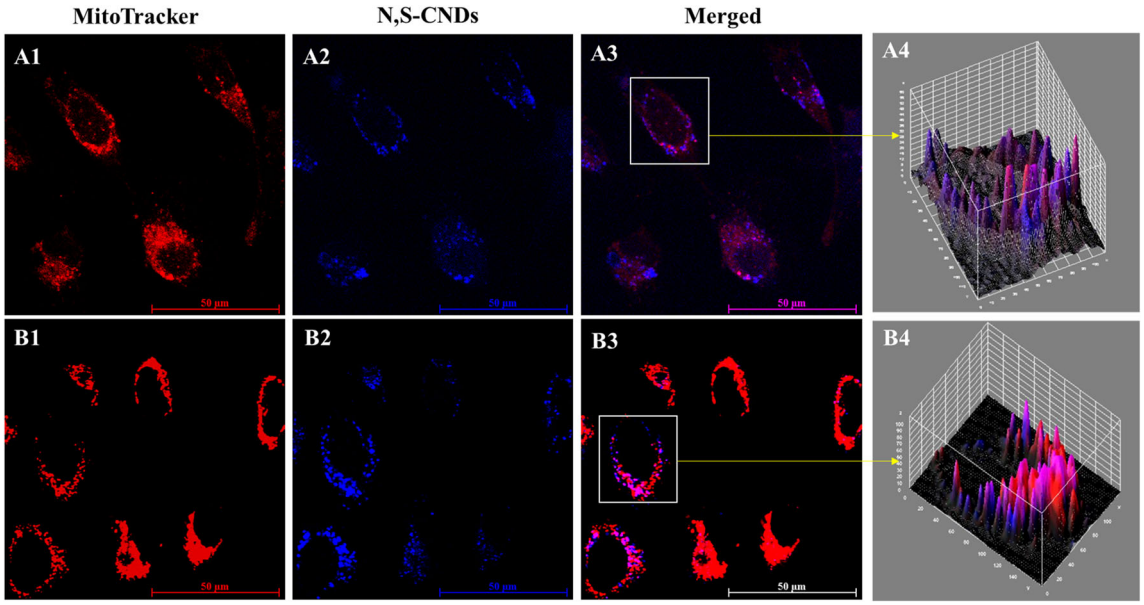

Figure 6 Confocal imaging subcellular localization of the N,S-CNDs (Ex. 405 nm) and MitoTracker (Ex. 532 nm) in two cell lines **a1**–**a4** EA.hy and **b1**–**b3** A549 with magnification of 60X. **a3** and **b3** the merged cell images of MitoTracker and N,S-CNDs (**a4**, **b4**) are 3D images of the selected cells show the overlap of MitoTracker and N,S-CNDs staining at the mitochondria.

redox signaling, because majority of ROS generation within the mitochondria occurs at the electron transport chain located on the mitochondrial membrane during the process of oxidative phosphorylation [58]. Indeed, the subcellular location of the CNDs in cells indicates more N,S-CNDs stained to mitochondria of EA.hy926 cells than A549 cells.

The findings in this work are of great significance, particularly compared to biological sulfur-containing compounds, such as cysteine, taurine, methionine, glutathione (GSH), N-acetylcysteine (NAC) and thioredoxin, which demonstrate antioxidant properties in cells [65]. Some other sulfur-containing NPs have shown strong antibacterial efficacy, e.g., nano-iron sulfides [66]. The precursor molecule, lipoic acid, is recognized as a powerful antioxidant involved in the NADPH redox reaction for inhibiting ROS generation by either quenching of ROS, chelating redox metals Cu(II) or Fe(II) and/or repairing oxidized proteins [67]. However, the entity of lipoic acid does not exist after the hydrothermal process for the N,S-CND synthesis; hence, it losses biological antioxidant capacity in cells.

In light of the structural composites of the N,S-CNDs and above described experimental results, the mechanism of oxidative effect is discussed as follow. A previous study suggested that positive charged CNDs by functionalizing polyethylenimine (PEI) enter into the cells by endocytosis, thus interact with nuclear membrane and bind to DNA, which induces ROS generation [35]. However, the polyethylene glycol (PEG) functionalized CNDs had insignificant effect on ROS generation. This mechanism of the ROS induction seems not applicable to the N,S-CNDs, because of the different surface structures, namely functional groups and composition, and the zero Zeta potential of the N,S-CNDs. In addition, one type of N-doped CNDs (without sulfur doping) developed in our laboratory, in contrast, shows antioxidation capacity in vitro in the two same cell lines (not shown here). This observation is also consistent with the antioxidation results of the biomass-derived CNDs containing nitrogen by Das et al. [27, 28]. Comparing these results to our findings of the N,S-CNDs, one can conclude that the sulfur in the CNDs plays an important role in regulating the ROS production in the two cells. While the N,S-CNDs present capacity of free radical scavenging in physicochemical environment and the S induced Stone–Wales defects and the polarizability act important roles [24, 68], the interplay of N,S-CNDs in the cells for ROS production is different. Researchers have identified at least 11 sites at complex I and complex III of the electron transport chain in mitochondria where the leakage of electrons may happen leading to partial reduction of oxygen to form superoxide (O_2^-), and subsequently dismutated

to hydrogen peroxide (H_2O_2) by two superoxide dismutase 1 and 2 [58, 69]. It is plausible that the N,S-CNDs interact with proteins in complex I and III by ligand interaction in the membrane of mitochondria [70], especially the metal–sulfur clusters in the complexes are reported to be responsible for ROS generation with dysfunction induced by external factors [71]. However, a further research with focus on examining the molecular level intracellular interactions of the CNDs within the cells, such as the complex proteins in mitochondria regarding the redox signing process, and potential interactions with NADPH oxidase for ROS is needed.

Conclusions

In summary, the N,S-doping CNDs show increased capacity for free radical scavenging in physicochemical environment, but the effect on oxidative stress in two types of living cells (EA.hy926 and A549 cell) is opposite. The N,S-CNDs actually present prooxidant effect by inducing more ROS generation by the cellular H_2O_2 and O_2^- measurement. The normal cell line EA.hy926 is more sensitive to the CNDs treatment at low concentration than the cancer cell line A549 in terms of the amount of ROS generation and the cell viability, suggesting that cell type does affect the toxicity study of nanoparticles. The observation of the localization of the N,S-CNDs at the mitochondria and the mitochondrial membrane potential increment with the treatment of the CNDs in the two cell lines suggests that there are interactions between the N,S-CNDs and mitochondria membrane, plausibly engaging ligand interactions between the sulfur functional groups of the CNDs with complexes in the electron transportation chain. This work opens a revenue to study the roles of structure–functional groups of CNDs in the cells for oxidative stress and other biological effects such as intracellular translocation and delivery, biocompatibility and toxicity.

Acknowledgements

The authors acknowledge the support of US NSF (No. 1832134). This work was performed at the JSNN, a member of South Eastern Nanotechnology Infrastructure Corridor (SENIC) and National Nanotechnology Coordinated Infrastructure (NNCI), which is supported by the National Science Foundation (ECCS-1542174).

Compliance with ethical standards

Conflict of interest No potential conflict of interest was reported by the authors.

References

[1] Zrazhevskiy P, Sena M, Gao X (2010) Designing multifunctional quantum dots for bioimaging, detection, and drug delivery. Chem Soc Rev 39:4326–4354

[2] Thomas CR, Ferris DP, Lee J-H et al (2010) Noninvasive remote-controlled release of drug molecules in vitro using magnetic actuation of mechanized nanoparticles. J Am Chem Soc 132:10623–10625

[3] Wolfbeis OS (2015) An overview of nanoparticles commonly used in fluorescent bioimaging. Chem Soc Rev 44:4743–4768

[4] Sun T, Zhang YS, Pang B, Hyun DC, Yang M, Xia Y (2014) Engineered nanoparticles for drug delivery in cancer therapy. Angew Chem Int Ed 53:12320–12364

[5] Panwar N, Soehartono AM, Chan KK et al (2019) Nanocarbons for biology and medicine: sensing, imaging, and drug delivery. Chem Rev 119:9559–9656

[6] Zhang D, Ye Z, Wei L, Luo H, Xiao L (2019) Cell membrane-coated porphyrin metal–organic frameworks for cancer cell targeting and o2-evolving photodynamic therapy. ACS Appl Mater Interfaces 11:39594–39602

[7] Lewinski N, Colvin V, Drezek R (2008) Cytotoxicity of nanoparticles. Small 4:26–49

[8] Manna SK, Sarkar S, Barr J et al (2005) Single-walled carbon nanotube induces oxidative stress and activates nuclear transcription factor-κb in human keratinocytes. Nano Lett 5:1676–1684

[9] Monteiro-Riviere NA, Inman AO (2006) Challenges for assessing carbon nanomaterial toxicity to the skin. Carbon 44:1070–1078

[10] Park MVDZ, Neigh AM, Vermeulen JP et al (2011) The effect of particle size on the cytotoxicity, inflammation, developmental toxicity and genotoxicity of silver nanoparticles. Biomaterials 32:9810–9817

[11] Chong Y, Ge C, Yang Z et al (2015) Reduced cytotoxicity of graphene nanosheets mediated by blood-protein coating. ACS Nano 9:5713–5724

[12] Soenen SJ, Parak WJ, Rejman J, Manshian B (2015) (Intra)cellular stability of inorganic nanoparticles: effects on cytotoxicity, particle functionality, and biomedical applications. Chem Rev 115:2109–2135

[13] Wick P, Manser P, Limbach LK et al (2007) The degree and kind of agglomeration affect carbon nanotube cytotoxicity. Toxicol Lett 168:121–131

[14] Cui W, Li J, Zhang Y, Rong H, Lu W, Jiang L (2012) Effects of aggregation and the surface properties of gold nanoparticles on cytotoxicity and cell growth. Nanomedicine 8:46–53

[15] Zhang J, Yu S-H (2016) Carbon dots: large-scale synthesis, sensing and bioimaging. Mater Today 19:382–393

[16] Ge L, Pan N, Jin J et al (2018) Systematic comparison of carbon dots from different preparations—consistent optical properties and photoinduced redox characteristics in visible spectrum and structural and mechanistic implications. J Phys Chem C 122:21667–21676

[17] Xu X, Ray R, Gu Y et al (2004) Electrophoretic analysis and purification of fluorescent single-walled carbon nanotube fragments. J Am Chem Soc 126:12736–12737

[18] Mintz KJ, Zhou Y, Leblanc RM (2019) Recent development of carbon quantum dots regarding their optical properties, photoluminescence mechanism, and core structure. Nanoscale 11:4634–4652

[19] Wang Y, Hu A (2014) Carbon quantum dots: synthesis, properties and applications. J Mater Chem C 2:6921–6939

[20] Li H, Kang Z, Liu Y, Lee S-T (2012) Carbon nanodots: synthesis, properties and applications. J Mater Chem 22:24230–24253

[21] Xiao L, Sun H (2018) Novel properties and applications of carbon nanodots. Nanosc Horiz 3:565–597

[22] Wang Q, Huang X, Long Y et al (2013) Hollow luminescent carbon dots for drug delivery. Carbon 59:192–199

[23] Das R, Bandyopadhyay R, Pramanik P (2018) Carbon quantum dots from natural resource: a review. Mater Today Chem 8:96–109

[24] Zhang W, Chavez J, Zeng Z et al (2018) Antioxidant capacity of nitrogen and sulfur codoped carbon nanodots. ACS Appl Nano Mater 1:2699–2708

[25] Zhang W, Zeng Z, Wei J (2017) Electrochemical study of dpph radical scavenging for evaluating the antioxidant capacity of carbon nanodots. J Phys Chem C 121:18635–18642

[26] Ji Z, Sheardy A, Zeng Z et al (2019) Tuning the functional groups on carbon nanodots and antioxidant studies. Molecules 24:152

[27] Das B, Pal P, Dadhich P, Dutta J, Dhara S (2019) In vivo cell tracking, reactive oxygen species scavenging, and antioxidative gene down regulation by long-term exposure of biomass-derived carbon dots. ACS Biomater Sci Eng 5:346–356

[28] Das B, Dadhich P, Pal P, Srivas PK, Bankoti K, Dhara S (2014) Carbon nanodots from date molasses: new nanolights for the in vitro scavenging of reactive oxygen species. J Mater Chem B 2:6839–6847

[29] Wei X, Li L, Liu J et al (2019) Green synthesis of fluorescent carbon dots from gynostemma for bioimaging and antioxidant in zebrafish. ACS Appl Mater Interfaces 11:9832–9840

[30] Wang L, Li B, Li L et al (2017) Ultrahigh-yield synthesis of n-doped carbon nanodots that down-regulate ROS in zebrafish. J Mater Chem B 5:7848–7860

[31] Durantie E, Barosova H, Drasler B et al (2018) Carbon nanodots: opportunities and limitations to study their biodistribution at the human lung epithelial tissue barrier. Biointerphases 13:06D404

[32] Christensen IL, Sun Y-P, Juzenas P (2011) Carbon dots as antioxidants and prooxidants. J Biomed Nanotechnol 7:667–676

[33] Chong Y, Ge C, Fang G et al (2016) Crossover between anti- and pro-oxidant activities of graphene quantum dots in the absence or presence of light. ACS Nano 10:8690–8699

[34] Chen J, Dou R, Yang Z et al (2016) The effect and fate of water-soluble carbon nanodots in maize (*Zea mays* l.). Nanotoxicology 10:818–828

[35] Havrdova M, Hola K, Skopalik J et al (2016) Toxicity of carbon dots—effect of surface functionalization on the cell viability, reactive oxygen species generation and cell cycle. Carbon 99:238–248

[36] Xu Z-Q, Lan J-Y, Jin J-C, Dong P, Jiang F-L, Liu Y (2015) Highly photoluminescent nitrogen-doped carbon nanodots and their protective effects against oxidative stress on cells. ACS Appl Mater Interfaces 7:28346–28352

[37] Nie H, Li M, Li Q et al (2014) Carbon dots with continuously tunable full-color emission and their application in ratiometric pH sensing. Chem Mater 26:3104–3112

[38] Zhang B-X, Gao H, Li X-L (2014) Synthesis and optical properties of nitrogen and sulfur co-doped graphene quantum dots. New J Chem 38:4615–4621

[39] Deng Y, Zhao D, Chen X, Wang F, Song H, Shen D (2013) Long lifetime pure organic phosphorescence based on water soluble carbon dots. Chem Commun 49:5751–5753

[40] Dong Y, Pang H, Yang HB et al (2013) Carbon-based dots co-doped with nitrogen and sulfur for high quantum yield and excitation-independent emission. Angew Chem Int Ed 52:7800–7804

[41] Zeng Z, Zhang W, Arvapalli DM et al (2017) A fluorescence-electrochemical study of carbon nanodots (CNDs) in bio- and photoelectronic applications and energy gap investigation. Phys Chem Chem Phys 19:20101–20109

[42] van Meerloo J, Kaspers GJL, Cloos J (2011) In: Cree IA (ed) Cancer cell culture: methods and protocols. Humana Press, Totowa

[43] Nel A, Xia T, Maedler L, Li N (2006) Toxic potential of materials at the nanolevel. Science 311:622–627
[44] Zuberek M, Grzelak A (2018) In: Saquib Q, Faisal M, Al-Khedhairy AA, Alatar AA (eds) Cellular and molecular toxicology of nanoparticles. Springer, Cham
[45] McCord JM (2000) The evolution of free radicals and oxidative stress. Am J Med 108:652–659
[46] Circu ML, Aw TY (2010) Reactive oxygen species, cellular redox systems, and apoptosis. Free Radic Biol Med 48:749–762
[47] Schieber M, Chandel NS (2014) ROS function in redox signaling and oxidative stress. Curr Biol 24:R453–R462
[48] Sena LA, Chandel NS (2012) Physiological roles of mitochondrial reactive oxygen species. Mol Cell 48:158–167
[49] Reczek CR, Chandel NS (2015) Ros-dependent signal transduction. Curr Opin Cell Biol 33:8–13
[50] Beckman K, Ames B (1998) The free radical theory of aging matures. Physiol Rev 78:547–581
[51] Finkel T, Holbrook NJ (2000) Oxidants, oxidative stress and the biology of ageing. Nature 408:239–247
[52] Haigis MC, Yankner BA (2010) The aging stress response. Mol Cell 40:333–344
[53] Fukumura H, Sato M, Kezuka K et al (2012) Effect of ascorbic acid on reactive oxygen species production in chemotherapy and hyperthermia in prostate cancer cells. J Physiol Sci 62:251–257
[54] Chen Q, Wang Q, Zhu J, Xiao Q, Zhang L (2018) Reactive oxygen species: key regulators in vascular health and diseases. Br J Pharmacol 175:1279–1292
[55] Valentine JS, Wertz DL, Lyons TJ, Liou L-L, Goto JJ, Gralla EB (1998) The dark side of dioxygen biochemistry. Curr Opin Chem Biol 2:253–262
[56] Halliwell B (1991) Reactive oxygen species in living systems: source, biochemistry, and role in human disease. Am J Med 91:S14–S22
[57] Li X, Fang P, Mai J, Choi ET, Wang H, Yang X-f (2013) Targeting mitochondrial reactive oxygen species as novel therapy for inflammatory diseases and cancers. J Hematol Oncol 6:19
[58] Brand MD (2016) Mitochondrial generation of superoxide and hydrogen peroxide as the source of mitochondrial redox signaling. Free Radic Biol Med 100:14–31
[59] Madamanchi Nageswara R, Runge Marschall S (2007) Mitochondrial dysfunction in atherosclerosis. Circ Res 100:460–473
[60] Suski J, Lebiedzinska M, Bonora M, Pinton P, Duszynski J, Wieckowski MR (2018) In: Palmeira CM, Moreno AJ (eds) Mitochondrial bioenergetics: methods and protocols. Springer, New York
[61] Hua X-W, Bao Y-W, Chen Z, Wu F-G (2017) Carbon quantum dots with intrinsic mitochondrial targeting ability for mitochondria-based theranostics. Nanoscale 9:10948–10960
[62] Gao G, Jiang Y-W, Yang J, Wu F-G (2017) Mitochondria-targetable carbon quantum dots for differentiating cancerous cells from normal cells. Nanoscale 9:18368–18378
[63] Cao L, Wang X, Meziani MJ et al (2007) Carbon dots for multiphoton bioimaging. J Am Chem Soc 129:11318–11319
[64] Zhang D, Wei L, Zhong M, Xiao L, Li H-W, Wang J (2018) The morphology and surface charge-dependent cellular uptake efficiency of upconversion nanostructures revealed by single-particle optical microscopy. Chemical Science 9:5260–5269
[65] Fleischauer AT, Arab L (2001) Garlic and cancer: a critical review of the epidemiologic literature. J Nutr 131:1032S–1040S
[66] Xu Z, Qiu Z, Liu Q et al (2018) Converting organosulfur compounds to inorganic polysulfides against resistant bacterial infections. Nat Commun 9:3713
[67] Packer L, Suzuki YJ (1993) Vitamin e and alpha-lipoate: role in antioxidant recycling and activation of the nf-κb transcription factor. Mol Aspects Med 14:229–239
[68] Zhang L, Niu J, Li M, Xia Z (2014) Catalytic mechanisms of sulfur-doped graphene as efficient oxygen reduction reaction catalysts for fuel cells. J Phys Chem C 118:3545–3553
[69] Goncalves RLS, Quinlan CL, Perevoshchikova IV, Hey-Mogensen M, Brand MD (2015) Sites of superoxide and hydrogen peroxide production by muscle mitochondria assessed ex vivo under conditions mimicking rest and exercise. J Biol Chem 290:209–227
[70] Weiss MJ, Wong JR, Ha CS et al (1987) Dequalinium, a topical antimicrobial agent, displays anticarcinoma activity based on selective mitochondrial accumulation. Proc Natl Acad Sci USA 84:5444–5448
[71] Zorov DB, Juhaszova M, Sollott SJ (2014) Mitochondrial reactive oxygen species (ROS) and ROS-induced ros release. Physiol Rev 94:909–950